through the thicker barrier. In this situation, only the excited states above the ground-state electrochemical potential are observed. For equal tunnel barriers, tunneling out of the dot from excited states below the ground-state electrochemical potential can also be measured; see (*2*). Note that for a thick enough entrance barrier we can assume relaxation to the ground state between tunneling out and tunneling into the dot of the next electron.

9. See, for example, J. J. Palacios, L. Martin-Moreno, G. Chiappe, E. Louis, C. Tejedor, *Phys. Rev. B* **50**, 5760, (1994); for more references see the review by N. F. Johnson, *J. Phys. Condens. Matter* **7**, 965 (1995).
10. V. Fock, *Z. Phys*. **47**, 446 (1928); C. G. Darwin, *Proc. Cambridge Philos. Soc*. **27**, 86 (1930).
11. We believe that the smaller slopes in the experimental data of Fig. 5 for $B > \sim 7$ T are due to a changing confinement potential because screening from the leads is modified by the formation of Landau levels in the leads. This is also reflected in the changing stripe width at high *B*.
12. G. Thurner, H. Herold, H. Ruder, G. Schlicht, G. Wunner, *Phys. Lett*. **89A**, 133 (1982).
13. M. Wagner, U. Merkt, A. V. Chaplik, *Phys. Rev. B* **45**, 1951 (1992).
14. B. Su, V. J. Goldman, J. E. Cunningham, *ibid*. **46**, 7644 (1992); R. C. Ashoori *et al*., *Phys. Rev. Lett*. **71**, 613 (1993); T. Schmidt *et al*., *Phys. Rev. B* **51**, 5570 (1995).
15. For details of the calculation see M. Eto, *Jpn. J. Appl. Phys*. **36**, 3924 (1997). In the numerically exact calculations, every electron is assumed to occupy one of the lowest 15 single-particle states at $B = 0$. The strength of the Coulomb interaction is fixed such that $e^2/\varepsilon\sqrt{\hbar/m^*\omega_o} = \hbar\omega_o$ (ε is the permittivity). (Interactions between electrons in the dot and in the leads are neglected.) The calculated results indicate that the many-body states consist of one main configuration [two main configurations for $N = 3$ and $(S,M) = (\frac{1}{2},2)$] and several small contributions from other configurations. The depicted configurations in Fig. 3 overlap by ~70% or more with the many-body ground states (the spin-polarized states overlap by more than 95%).
16. For a theoretical analyses of the $N = 2$ excitation spectrum, see, for example, D. Pfannkuche, R. R. Gerhardts, P. A. Maksym, V. Gudmundsson, *Physica B* **189**, 6 (1993).
17. Also for $N \sim 100$ quantum dots the excitation spectra of N and $N + 1$ can be strongly correlated, as observed recently by D. R. Stewart *et al*. [D. R. Stewart, D. Sprinzak, C. M. Marcus, C. I. Duruöz, J. S. Harris Jr., *Science* **278**, 1784 (1997)].
18. We thank R. J. van der Hage, J. Janssen, Y. Kervennic, J. E. Mooij, S. K. Nair, L. L. Sohn, Y. Tokura, and T. Uesugi for help and discussions. Supported by the Dutch Foundation for Fundamental Research on Matter. L.P.K. was supported by the Royal Netherlands Academy of Arts and Sciences.

21 July 1997; accepted 8 October 1997

Coupled Quantum Dots Fabricated by Cleaved Edge Overgrowth: From Artificial Atoms to Molecules

Gert Schedelbeck, Werner Wegscheider,*
Max Bichler, Gerhard Abstreiter

Atomically precise quantum dots of mesoscopic size have been fabricated in the gallium arsenide–aluminum gallium arsenide material system by cleaved edge overgrowth, with a high degree of control over shape, composition, and position. The formation of bonding and antibonding states between two such "artificial atoms" was studied as a function of quantum dot separation by microscopic photoluminescence (PL) spectroscopy. The coupling strength within these "artificial molecules" is characterized by a systematic dependence of the separation of the bonding and antibonding levels, and of the PL linewidth, on the "interatomic" distance. This model system opens new insights into the physics of coupled quantum objects.

Over the last 5 years, quantum dots (QDs)—boxes in which charge carriers are quantum-confined in three dimensions—have been realized in semiconductors (*1*–*11*). Although these QDs are commonly part of a single crystalline solid, their properties are in many ways analogous to those of atoms (*10*); a "shell-like" energy staircase for single-electron charging (*11*) and extremely narrow homogeneous linewidths in optical spectra have been observed (*6*). The growing interest in QD systems is not only of a fundamental nature but is strongly driven by applications such as semiconductor laser devices, where discrete energy level schemes should be advantageous in many respects (*12*).

A diverse range of technologies, including high-resolution electron beam lithography and focused laser beam writing, have been implemented to fabricate such "artificial atoms" from layers prepared by molecular beam epitaxy (MBE); such layers often serve as starting material because quantum confinement along the growth direction can be readily achieved (*1*, *2*). Unfortunately, QDs confining excitons of high optical quality whose emission is governed by narrow "atom-like" lines must be prepared differently. In the GaAs-AlGaAs material system, their size must be in the 10-nm range, the equivalent of the hydrogen-like Bohr orbit for excitons. The latter represent quantized excitations in a semiconductor in the form of electrostatically bound electron hole pairs.

To date, the realization of such QDs has relied on monolayer thickness fluctuations of thin quantum wells (QWs) (*3*–*6*) or on spontaneous island formation during strained layer epitaxy (*7*–*9*). These structures have the advantage that they contain few crystal imperfections, which are inevitably accompanied by a high number of nonradiative recombination centers. However, as a consequence of the inherent randomness in the formation process of ensembles of such natural and self-organized QDs, they differ in size and shape, and their position is not under precise experimental control. Therefore, highly local spectroscopic techniques are essential to extract the properties of individual objects. The long-standing question of whether the analogy between QDs and artificial atoms can be taken even further—that is, whether coupled QDs act like coupled atoms in a molecule (*13*)—must therefore be answered in a different kind of experiment.

Here, we report on the fabrication of individual and coupled QDs of high optical quality whose size, shape, and position are completely engineered by the fabrication process. Starting from an artificial atom characterized by a homogeneous linewidth as narrow as 70 μeV (full width at half maximum, FWHM) in optical emission spectra, the formation of an "artificial molecule" can be observed as the coupling strength is gradually increased. As coupling between two QDs is introduced, the sharp resonance resulting from ground-state exciton transitions of an isolated dot splits into a pair of lines. The splitting as well as the peak widths systematically increase with increasing coupling strength.

This scenario of an exciton bound to two quantum-mechanically coupled QDs can be compared to the synthesis of a positively charged hydrogen molecule H_2^+ from an electron and two protons; such a system can be described in the framework of elementary quantum mechanics by the formation of bonding and antibonding states. In contrast to previous work on coupled Coulomb islands, which were explained in terms of classical interdot capacitance coupling (*2*), the excitonic states in our QDs are quantum-mechanically coupled and can be thought of as a coherent wave that is delocalized over the two dots. Such widely adjustable, coherently coupled QDs seem to be ideally suited for fundamental studies in a regime that is inaccessible to experiments on real atoms.

Our sample design is based on quantum

Walter Schottky Institut, Technische Universität München, Am Coulombwall, D-85748 Garching, Germany.

*To whom correspondence should be addressed. E-mail: wegscheider@wsi.tu-muenchen.de

confinement of excitons to two, one, and zero dimensions, which is realized by twofold application of cleaved edge overgrowth (CEO), a method described in detail in (*14*). The structure investigated here makes explicit use of atomic control of both the size and position of CEO QDs, which arise from three MBE growth steps (Fig. 1). The layer sequence of the first growth step consists of three double QWs (QW$_{1A}$-QW$_{1B}$, QW$_{1C}$-QW$_{1D}$, and QW$_{1E}$-QW$_{1F}$) followed by a single QW (QW$_{1G}$) embedded in Al$_{0.3}$Ga$_{0.7}$As barrier material. All GaAs QW layers are 7 nm wide and are overgrown after cleavage along the two ⟨110⟩ directions by another 7-nm-wide QW and an Al$_{0.3}$Ga$_{0.7}$As barrier. This leads to the formation of three coupled, T-shaped QD systems and one individual T-shaped QD, which are connected by the single, T-shaped quantum wire QWR$_{23}$ (inset, Fig. 2). The barriers separating the two QDs, which form coupled QD systems, are 15, 30, and 60 nm wide, respectively. This spatial distance between the QDs adjusts the coupling strength of the zero-dimensional QD levels. The center-to-center distance from the individual QD to the first and the following coupled QD systems was chosen to be 800 nm. In this way, spatial isolation of the individual objects is possible without the use of non–diffraction-limited probes, as in near-field optical microscopy (*4*, *6*). This series of QDs was designed to monitor subsequent phases in the formation of artificial molecules out of artificial atoms in a single sample and was investigated by means of conventional, diffraction-limited microphotoluminescence (μPL) spectroscopy combining high spatial and spectral resolution (*15*).

In the μPL spectrum from an individual T-shaped QD, recorded from the ($\bar{1}$10) surface resulting after the last growth step, not only the QD but also the adjacent QWs and QWRs are excited and can be spectrally resolved (Fig. 2). Although most of the excitons are photoexcited in the QWs and QWRs, the observed PL response is dominated by a single sharp line at an energy of 1565.9 meV, which we attribute to recombination of zero-dimensional excitons in the QD. Emission from excitons recombining in the QWs is observed at energies of ~1590 meV (QW$_{1G}$) and 1583 meV (QW$_2$/QW$_3$) (*16*). The relatively strong response from the QWRs at ~1571 meV results from efficient collection of the emission from QWR$_{1G2}$ along its length within the excitation volume. As a result of the high spatial resolution of our μPL setup, the QWR emission (and, to a lesser extent, the QW emission) exhibits the sharp lines that are characteristic for exciton localization at monolayer fluctuations and are a subject of current research (*17*). The unambiguous assignment of the peaks to the different low-dimensional structures in our sample follows from a detailed three-dimensional μPL mapping using various geometries. The linewidth of the individual T-shaped QD of FWHM = 70 μeV is comparable to those observed in atomic spectra, and thus directly reflects the discreteness of the density of states resulting from three-dimensional quantum confinement. The ground-state wavefunction of excitons confined to CEO QDs has been calculated (*18*). An energy decrease of the QD excitonic ground state with respect to the corresponding QWR state of ~6 meV was found for 7-nm-wide QWs, which is in good agreement with our experimentally determined value of ~5 meV.

Figure 3 shows the spectral image of a linescan along QWR$_{23}$ on an enlarged energy scale together with a schematic drawing of the sample geometry. At the right-hand side, the single line originating from excitons recombining within the individual QD can be seen at an energy of 1565.9 meV. Moving the excitation and detection window to the coupled QDs, a series of sharp double peaks appears. The spatial positions of the intensity maxima of all peaks exactly coincide with the designed positions of our

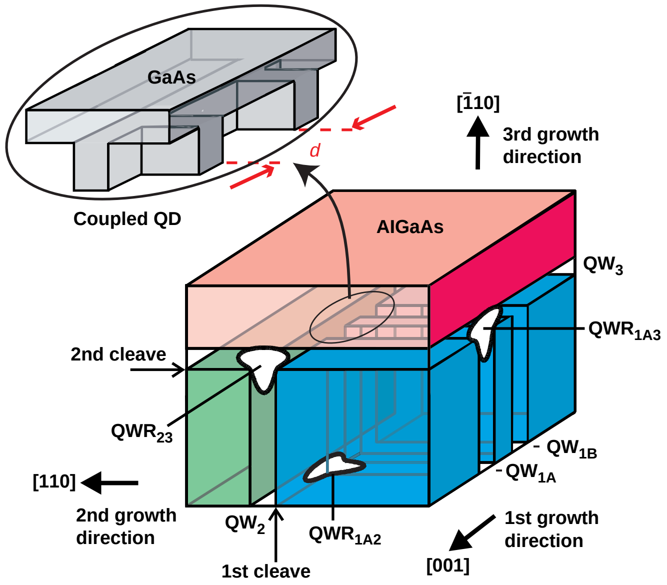

Fig. 1. Schematic illustration of a T-shaped, coupled QD structure. First, GaAs quantum wells (QW$_{1A}$, QW$_{1B}$) separated by Al$_{0.3}$Ga$_{0.7}$As barriers are grown along the [001] direction (blue layers). The sample is then cleaved two times in situ, and the fresh, atomically smooth (110) and ($\bar{1}$10) cleavage planes are subsequently overgrown with single quantum wells (QW$_2$ and QW$_3$) and Al$_{0.3}$Ga$_{0.7}$As barriers (green and red layers). At each intersection of two QWs, a T-shaped quantum wire (QWR) forms (*20*–*23*), which provides exciton confinement in two dimensions. This results in the formation of three distinct types of QWRs. The T-shaped contours schematically represent lines of constant probability for excitons confined to QWR$_{1A2}$, QWR$_{1A3}$, and QWR$_{23}$. Each intersection of three QWs (and consequently QWRs) constitutes a QD (*24*), thereby confining excitons in all three dimensions. The ground-state energy of such T-shaped QDs is further lowered with respect to the QWR because of additional confinement relaxation by the third QW.

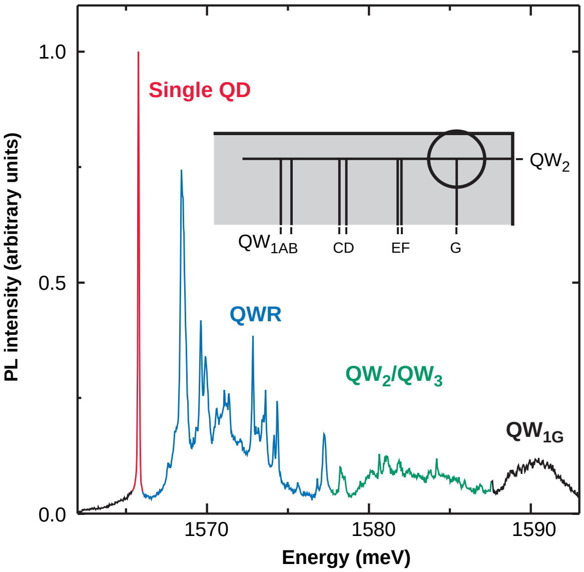

Fig. 2. Microphotoluminescence (μPL) spectrum (E_{exc} = 1601 meV) taken at the position of the individual QD from the ($\bar{1}$10) sample surface resulting after the third growth step. The cutaway schematic of the sample along the plane of QW$_3$ (inset) shows the QW intersections at which the three coupled QDs (QD separation not to scale) and one individual QD form. The excitation and detection range is indicated by the superimposed circle.

individual and coupled QD systems and are therefore separated by 800 nm. This clear correlation of the sharp lines with position again confirms that they indeed originate from excitonic recombination in the CEO QDs. The energetic spread of the peaks in the range of 1 to 2 meV can be well described by monolayer thickness fluctuations in the overgrown QWs. However, the wavefunction of the coupled QDs probes only a very short part of the constituting QWs with respect to the length scale of monolayer fluctuations and coupling between almost identical objects can be studied.

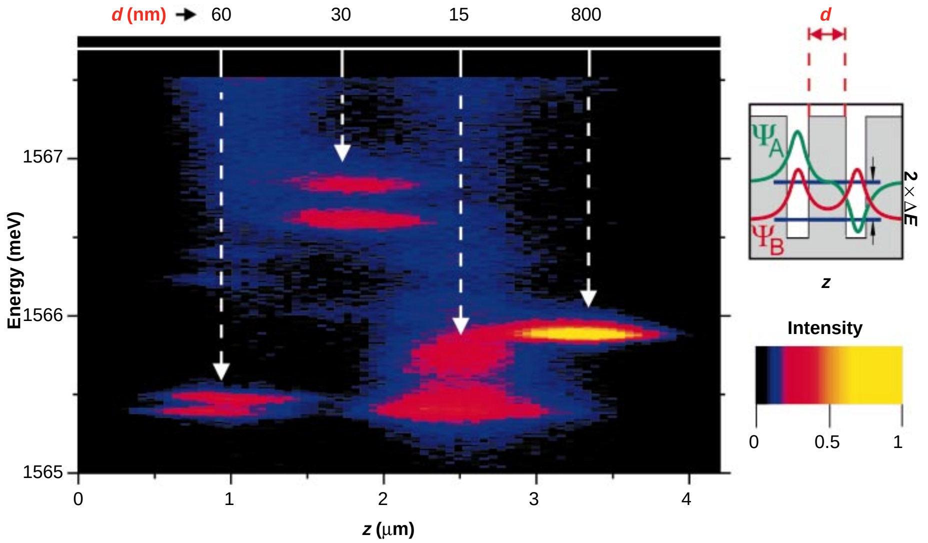

Fig. 3. Spectral image resulting from a high-resolution μPL linescan ($E_{\mathrm{exc}} = 1588$ meV) along QWR_{23}, which connects all QDs (denoted as the *z* direction), taken from the $(\bar{1}10)$ sample surface. The spatial position of the coupled QDs and the single QD are given by the scale drawing of the QW intersections along the top of the image. These positions coincide with the spatial positions of intensity maxima in the spectra at 0.9, 1.7, 2.5, and 3.3 μm, as indicated by the dashed lines and arrows. The spatial width of the peaks is limited by the spatial resolution of the μPL setup. The separations (*d*) of the QDs forming coupled systems are given at the corresponding QW intersections. The one-dimensional potential profile for excitons in the coupled systems, the resulting bonding (Ψ_B) and antibonding wavefunctions (Ψ_A), and the energetic splitting $2 \times \Delta E$ of such a two-level system are shown in the inset.

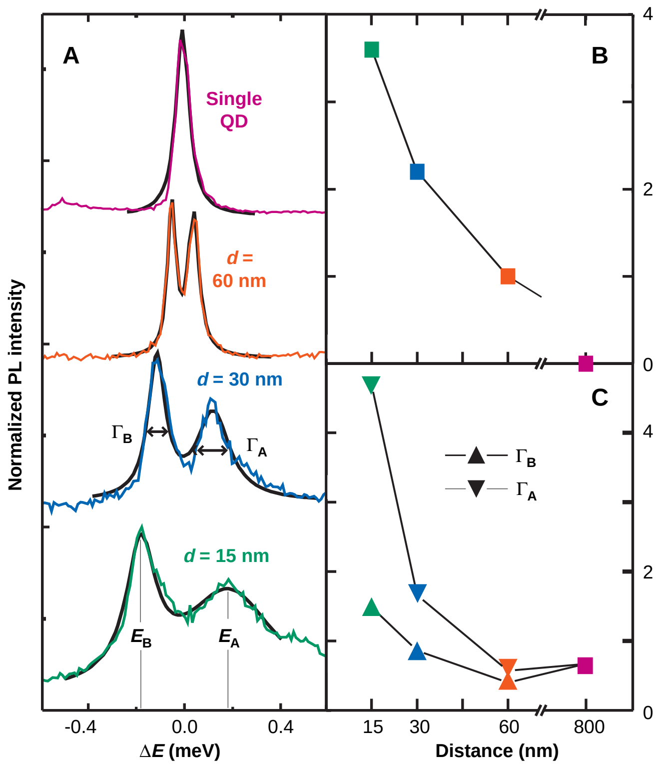

Fig. 4. (**A**) Selected μPL spectra from the linescan of Fig. 3 of the single QD and the coupled CEO QDs (at the positions marked by the arrows), plotted on a relative energy scale and offset vertically against each other for clarity. (**B**) Energetic splitting $2 \times \Delta E = E_A - E_B$ between the bonding and antibonding levels. (**C**) Linewidths of the two levels as a function of the QD distance. The solid lines in (B) and (C) are a guide for the eye; the colors of the symbols correspond to the colors used in (A) for each *d* value.

The appearance of two energetically distinct peaks from coupled QDs (Fig. 3) is clear evidence that their excitonic levels are coupled. Such a coupling is possible despite the QDs' separation of 15 to 60 nm, because the effective barrier height between the dots represented by QWR_{23} is only ~5 meV. The influence of coupling on the excitonic levels, on the order of 100 μeV, is small relative to the binding energy of an exciton confined to a CEO QD of more than 10 meV (*18*). Therefore, the exciton is considered as one particle whose internal structure is not affected by coupling. In analogy to the two coupled electronic levels of the H_2^+ molecule, the wavefunction Ψ of our system of two coupled excitonic dot levels can be approximated by the sum and difference of the wavefunctions of individual dots. These wavefunctions, Ψ_B and Ψ_A, correspond to the bonding and antibonding states (Fig. 3). From first-order perturbation theory, the energy levels of the coupled system can be written as $E_{B/A} = E_0 \mp \Delta E$, where E_0 is the energy level of an individual QD and ΔE is a matrix element that describes the energetic splitting $2 \times \Delta E$ caused by coupling. Following this argument, we assign the two energetically distinct PL lines of each coupled QD to emission from the bonding and antibonding energy levels, which are separated by $2 \times \Delta E$. Spectra from the QDs are shown on a relative energy scale in Fig. 4A to facilitate a more detailed discussion. The systematic dependence of the energetic splitting on the distance between the coupled QDs (Fig. 4B) further confirms our interpretation in terms of bonding and antibonding states. The observed enhancement of the energetic splitting with decreasing distance between the coupled QDs directly reflects the increasing coupling strength of the QD levels.

The optical emission from individual, naturally formed QDs with discrete energy levels is subject only to homogeneous line broadening and is therefore characterized by a Lorentzian line shape (*6*). In agreement with this result, the spectra of our QDs are well fitted with Lorentzians (black lines in Fig. 4A). This implies that the PL linewidths of the transitions corresponding to the bonding and antibonding states are lifetime-broadened. These linewidths increase systematically with increasing coupling strength (Fig. 4C). The broadening is especially pronounced for emission from the antibonding level. For the strongest coupled QD, the PL linewidth for emission from the antibonding level of 470 μeV is slightly larger than the energetic splitting of the levels. On the other hand, the PL linewidth corresponding to the bonding level of the most weakly coupled QDs is as low as the spectral resolution of our spectrometer, 40 μeV, a value comparable to the smallest linewidth reported so far (*6*). The decrease of the exciton lifetime for the antibonding state with increasing level separation can be described in a simple two-level picture involving acoustical phonon scattering from the upper state into the lower state (*19*). This would lead to a cubic dependence of this linewidth on the energy level separation, which is also observed experimentally.

CEO has proven to be a versatile method for the fabrication of zero-dimensional objects of well-defined size, shape, and position. The excellent optical quality, manifested in extremely narrow emission lines, and the high degree of homogeneity accessible with this method permit the precise tailoring of the quantum-mechanical coupling between these nanoscale structures. As an extension to this work, we propose the use of higher barriers, narrower QWs, and the incorporation of indium into the wells. All these measures should increase the binding energy of excitons to the QDs. The use of strained InGaAs QWs, in particular, is expected to enhance this binding energy drastically because the strain can be almost completely elastically relaxed at the intersections. This might open a route to experimental investigation of a variety of quantum mechanics textbook examples previously inaccessible by other means, such as going from artificial atoms to molecules to an artificial one-dimensional solid.

REFERENCES AND NOTES

1. K. Brunner *et al.*, *Phys. Rev. Lett.* **69**, 3216 (1992).
2. N. C. van der Vaart *et al.*, *ibid*. **74**, 4702 (1995); F. R. Waugh *et al.*, *ibid*. **75**, 705 (1995).
3. A. Zrenner *et al.*, *ibid.* **72**, 3382 (1994).
4. H. F. Hess, E. Betzig, T. D. Harris, L. N. Pfeiffer, K. W. West, *Science* **264**, 1740 (1994).
5. K. Brunner, G. Abstreiter, G. Böhm, G. Tränkle, G. Weimann, *Phys. Rev. Lett.* **73**, 1138 (1994).
6. D. Gammon, E. S. Snow, B. V. Shanabrook, D. S. Kratzer, D. Park, *ibid.* **76**, 3005 (1996); *Science* **273**, 87 (1996).
7. J.-Y. Marzin, J.-M. Gérard, A. Izraël, D. Barrier, G. Bastard, *Phys. Rev. Lett.* **73**, 716 (1994).
8. R. Leon, P. M. Petroff, D. Leonard, S. Fafard, *Science* **267**, 1966 (1995).
9. M. Grundmann *et al.*, *Phys. Rev. Lett.* **74**, 4043 (1995).
10. M. A. Kastner, *Phys. Today* **46**, 24 (January 1993); O. Klein *et al.*, *Phys. Rev. Lett.* **74**, 785 (1995); R. C. Ashoori *et al.*, *ibid.* **71**, 613 (1993); R. C. Ashoori, *Nature* **379**, 413 (1996).
11. S. Tarucha, D. G. Austing, T. Honda, R. J. van der Hage, L. P. Kouwenhoven, *Phys. Rev. Lett.* **77**, 3613 (1996).
12. Y. Arakawa and A. Yariv, *IEEE J. Quantum Electron.* **22**, 1887 (1986).
13. L. Kouwenhoven, *Science* **268**, 1440 (1995).
14. L. Pfeiffer *et al.*, *Appl. Phys. Lett.* **56**, 1697 (1990).
15. Light from a tunable dye laser was focused through a microscope objective lens (numerical aperture = 0.75, power density = 50 W cm^{-2}) onto the sample mounted in a He cryostat. Under such conditions, less than one exciton at a time is expected to be in the QDs. The emitted light was collected by the same objective lens and directed to a confocal imaging system, which defined a nearly diffraction-limited detection range of FWHM = 800 nm. The PL signal was dispersed with a triple-grating spectrometer (spectral resolution = 40 μeV) and detected with a cooled charge-coupled-device camera.
16. The PL energy of (110) QWs is red-shifted with respect to that of (001) QWs of identical thickness because of different heavy hole masses in these two directions.
17. J. Hasen *et al.*, *Nature* **390**, 54 (1997).
18. M. Grundmann and D. Bimberg, *Phys. Rev. B* **55**, 4054 (1997).
19. P. Platzman, personal communication.
20. Y. C. Chang, L. L. Chang, L. Esaki, *Appl. Phys. Lett.* **47**, 1324 (1985).
21. A. R. Gõni *et al.*, *ibid.* **61**, 1956 (1992).
22. W. Wegscheider *et al.*, *Phys. Rev. Lett.* **71**, 4071 (1993).
23. T. Someya, H. Akiyama, H. Sakaki, *ibid.* **74**, 3664 (1995); *ibid*. **76**, 2965 (1996).
24. W. Wegscheider, G. Schedelbeck, G. Abstreiter, M. Rother, M. Bichler, *ibid.* **79**, 1917 (1997).

25. We thank A. Zrenner for helpful discussions. Supported by the Deutsche Forschungsgemeinschaft in the framework of SFB 348 and the Bundesministerium für Bildung, Wissenschaft, Forschung, und Technologie through contract 01 BM 630/1.

13 August 1997; accepted 15 October 1997

Organically Modified Aluminosilicate Mesostructures from Block Copolymer Phases

Markus Templin, Achim Franck, Alexander Du Chesne,
Heike Leist, Yuanming Zhang, Ralph Ulrich, Volker Schädler,
Ulrich Wiesner*

Organically modified aluminosilicate mesostructures were synthesized from two metal alkoxides with the use of poly(isoprene-*b*-ethyleneoxide) block copolymers (PI-b-PEO) as the structure-directing molecules. By increasing the fraction of the inorganic precursors with respect to the polymer, morphologies expected from the phase diagrams of diblock copolymers were obtained. The length scale of the microstructures and the state of alignment were varied using concepts known from the study of block copolymers. These results suggest that the use of higher molecular weight block copolymer mesophases instead of conventional low–molecular weight surfactants may provide a simple, easily controlled pathway for the preparation of various silica-type mesostructures that extends the accessible length scale of these structures by about an order of magnitude.

Currently, a great deal of attention is being paid to the synthesis of complex inorganic materials with long-range order (*1*). Such materials could find applications in catalysis, membrane and separation technology, and molecular engineering (*2*). A typical approach is the use of organic structures formed through self-assembly as structure-directing agents. The final morphology is then determined by the cooperative organization of inorganic and organic molecular species into three-dimensionally structured arrays, a concept also discussed in the context of biomineralization (*3*). This strategy has already been successfully used in the preparation of inorganic mesoporous materials (*4*). Different pathways, where the driving forces of the cooperative organization are either ionic (*5*) or based on hydrogen bonds (*6*), have been described in vastly different concentration regimes (*7*). Pore sizes of 20 to 100 Å are commonly obtained in this way.

Here, we used block copolymers of higher molecular weight to make the transition from the small to the large mesoscopic regime (up to several tens of nanometers) of silica-type mesostructures. Bagshaw *et al.* previously used block-type low–molecular weight surfactants as templating agents to produce mesoporous molecular sieves (*6*). Higher molecular weight block copolymers have been used to stabilize inorganic metal or semiconductor nanoparticles (*8*). However, they all produce solid particles with morphologies never very far from spherical (*9*). An example of a different shape of inorganic material in a random-coil organic homopolymer is the synthesis of randomly distributed inorganic nanowires (*10*). Most recently, block copolymers have been used to control the growth of anisotropic inorganic crystals (*11*).

Block copolymer materials are similar to low–molecular weight nonionic surfactant solutions with respect to their general phase behavior (*12*). The phase diagrams of these materials have been elucidated by numerous experimental and theoretical studies (*13*). The combination of inorganic siliceous components in a hybrid material with block copolymers is appealing for various reasons.

Max-Planck-Institut für Polymerforschung, Postfach 3148, 55021 Mainz, Germany.

*To whom correspondence should be addressed.

Science

Coupled Quantum Dots Fabricated by Cleaved Edge Overgrowth: From Artificial Atoms to Molecules

Gert Schedelbeck, Werner Wegscheider, Max Bichler and Gerhard Abstreiter

Science **278** (5344), 1792-1795.
DOI: 10.1126/science.278.5344.1792

Science (print ISSN 0036-8075; online ISSN 1095-9203) is published by the American Association for the Advancement of Science, 1200 New York Avenue NW, Washington, DC 20005. The title *Science* is a registered trademark of AAAS.